WARHEAD PERFORMANCE CALCULATIONS FOR THREAT HAZARD ASSESSMENT

Andrew C. Victor
Victor Technology
1537 Fourth St., Suite 218
San Rafael, California 94901

INTRODUCTION

Measurements of warhead performance are expensive. The results are strongly dependent on details of warhead design, necessary economies at the measurement facility, and round-to-round variations. Therefore it is essential to have a capability to make warhead performance predictions in the earliest phases of weapon preliminary design. Methods presented here for predicting warhead performance, applicable for all levels of design, are derived from Victor Technology's prior experience in the assessment of warhead performance and are also useful for predicting fragment threats in hazard assessments. Although these methods are formally simple, they represent significant improvements over more simplistic methods often used.

The term "warhead performance" encompasses the "terminal effects" phase of munitions operational requirements. In general, this includes (1) fragment size distribution, spatial distribution, velocity, and fragment effects on specific targets; and (2) blast overpressure, impulse, and their effects on specific targets. For specialized warheads, there are other performance parameters; for example: Penetrator warheads must be able to perforate specified thicknesses of structural materials without preliminary initiation, structural failure, or other functional degradation; Shaped-charge warheads must produce jets conforming to design requirements for penetration of specific thicknesses of armor; and Underwater warheads must produce energetic gas bubbles that transfer energy to a water shock wave (a similar energy requirement exists for some penetrator warheads whose major damage mechanism is rapid pressure generation in interior ship or bunker compartments). Shaped charge design is a highly specialized field not represented in this paper, however Chanteret summarized simple design methods in a recent paper.[44]

Hydrodynamic codes, currently available, can produce detailed and instructive pictures of warhead performance effects as functions of time. However, warheads were being designed long before these codes and the computers they run on existed. The analytical methods that were developed in the two decades following World War II are used in this paper. These methods are based on combinations of data analysis and theory that agree well with data, and thus are generally as accurate as hydrocode methods and much faster in use. Exceptions occur for penetrator warheads for which hydrocode solutions give wave dynamics related to structural failure and unexpected initiation points in the penetrator during the impact and penetration process. For shaped charge jet warheads, hydrocodes can track two-dimensional collapse of the jet-forming cone driven by specific explosives, subsequent jet elongation and breakup, and penetration into targets. Shortly after the study upon which this paper is based was completed, Joseph Carleone's excellent book, *Tactical Missile Warheads*, became available,.[45] While this large book presents, for the first time in a single source, much of the information the present paper was written to include (and a great deal more), it does not cover the blast damage effects, which were derived from a unique combination of other books[14,16] and papers.[25] Carleone's book is unequivocally recommended to anyone who finds this brief paper useful.

WARHEAD CASE FRAGMENTATION

Fragment Size Distribution

Ordnance warheads are generally axisymetric. This reduces perfomance calculations to two dimensions. Warhead fragmentation is generally one of two types: natural fragmentation or controlled fragmentation. Natural fragmentation yields a random distribution of fragment sizes (masses) that can be described analytically. Controlled fragmentation creates fragments closely distributed around one or several specific sizes.

Several methods exist for producing controlled fragments. Preformed fragments are usually loaded into the warhead case with a specific size and shape and that is the form they retain during acceleration following warhead detonation. Fragment size can also be controlled by causing the shear induced failure of the warhead case to follow certain paths that result in one or more fragment sizes within close tolerances. Both scoring of the case and formed liners have been used for shear control.[1] Fragments formed by liner effects will tend to be a mixture of formed and natural fragments. Held has shown that the size distribution of this mixture can be treated analytically.[2]

The maximum velocity attained by fragments is relatively independent of the fragmentation mechanism, although Pearson's data (on 5-inch-diameter warheads) show that shear-controlled fragments (by scoring) are a little

1. REPORT DATE **AUG 1996**	2. REPORT TYPE	3. DATES COVERED **00-00-1996 to 00-00-1996**
4. TITLE AND SUBTITLE **Warhead Performance Calculations for Threat Hazard Assessment**		5a. CONTRACT NUMBER
		5b. GRANT NUMBER
		5c. PROGRAM ELEMENT NUMBER
6. AUTHOR(S)		5d. PROJECT NUMBER
		5e. TASK NUMBER
		5f. WORK UNIT NUMBER
7. PERFORMING ORGANIZATION NAME(S) AND ADDRESS(ES) **Victor Technology,1537 Fourth St., Suite 218,San Rafael,CA,94901**		8. PERFORMING ORGANIZATION REPORT NUMBER
9. SPONSORING/MONITORING AGENCY NAME(S) AND ADDRESS(ES)		10. SPONSOR/MONITOR'S ACRONYM(S)
		11. SPONSOR/MONITOR'S REPORT NUMBER(S)

12. DISTRIBUTION/AVAILABILITY STATEMENT
Approved for public release; distribution unlimited

13. SUPPLEMENTARY NOTES
See also ADM000767. Proceedings of the Twenty-Seventh DoD Explosives Safety Seminar Held in Las Vegas, NV on 22-26 August 1996.

14. ABSTRACT

15. SUBJECT TERMS

16. SECURITY CLASSIFICATION OF:			17. LIMITATION OF ABSTRACT	18. NUMBER OF PAGES	19a. NAME OF RESPONSIBLE PERSON
a. REPORT **unclassified**	b. ABSTRACT **unclassified**	c. THIS PAGE **unclassified**	**Same as Report (SAR)**	**19**	

faster (perhaps 5%), possibly because less energy is required to fragment the case.[1] One would expect this effect to disappear for large-diameter warheads that have longer fragment acceleration times.

For naturally fragmenting warheads, the Mott equation (1) has been in use for 50 years.[3] Refinements to the Mott equation, included below, have led to improved dependencies of fragment size distribution on warhead design parameters.

$$N(m) = (M/M_{ave}) \exp(-(m/\mu_j)^{1/j}) = \text{number of fragments larger than mass m} \qquad (1)$$

$$M_{ave} = 2 B^2 (t_o/d_i)^2 (t_o + d_i)^3 (1+0.5\ M/C) = \text{average fragment mass} \qquad (2)$$

$$\mu_j = M_{ave}/j! \quad \text{where j is the dimensionality} \qquad (3)$$

where: C = mass of explosive charge
  M = total mass of cylindrical section of case
  B = a function of the explosive and the case material in equation (2), the
      Gurney-Sarmousakis equation. As a rough approximation, for a mild steel
      case, B = 338.1/P_{CJ}, with the detonation pressure (P_{CJ}) in kbar.
  t_o = case thickness in inches
  d_i = case internal diameter (i.e., explosive diameter), inches

For cylindrical warheads of C/M < 2, the value of j = 2 is used. For very thin walls (i.e., C/M > 2), it has been observed that j = 1 agrees best with cylinder fragmentation tests. For very thick case walls, j = 3 may be necessary. The constant B obviously decreases with increasing detonation pressure (yielding smaller fragments); it also decreases with increasing case hardness.

The Magis equation (4) is also a popular alternative to the Gurney Sarmousakis equation.[4] For large cases (either larger diameter or thicker case walls), equation (4), when applied in equation (1), will give a smaller mass of maximum size fragment (m_{max}) and a larger total number of fragments than equation (2); for small cases, the reverse occurs.

$$M_{ave} = C_M (t_o\ d_i^{1/3})/(1 + 2\ C/M) = \text{Magis equation for average fragment mass} \qquad (4)$$

In this document, equation (2) to is used exclusively. The relationships of equations (2) or (4) to warhead design parameters permit a priori prediction of fragment size distribution.

Recent literature challenges some results obtained with the Mott equation. Held claims that an improved fit to natural-fragmentation data can be obtained using equation (5).[5]

$$M(n) = M [1 - \exp(-C_H\ n^\lambda)] \qquad (5)$$

where C_H and λ are both empirically determined constants, with C_H = constant $\sqrt{(d_i/t_o)}$ and of order 10^{-2} and λ of order 2/3. In equation (5), M(n) is the summed mass of the first (heaviest) n fragments. Held frequently finds it necessary to discard a few of the heaviest fragments in order to obtain a curve fit to data over the rest of the range.

Differentiating equation (5) gives

$$m(n) = M\ C_H\ \lambda\ n^{\lambda-1} \exp(-C_H\ n^\lambda) \qquad (6)$$

the approximate mass of the nth fragment. It is preferable to use exact difference values given by equation (5).

$$m(n) = M(n) - M(n-1) \qquad (7)$$

Strømsøe and Ingebrigtsen have applied a modified Mott formula, equation (8), which they claim avoids overestimation of the number of very large fragments.[6]

$$N(m) = (\mu_o/2\mu_k^2) (1 - \sin(\pi\ m/2m_{max})) \exp(-m^{1/2}/\mu_k) \text{ for } m < m_{max} \qquad (8)$$

$$N(m) = 0 \text{ for } m > m_{max}$$

The three parameters in equation (8) are obtained by curve fitting fragment data. The variables μ_o and μ_k in equation (8) are comparable in value to the similarly located variables M and M_{ave} in equation (1), although they may be up to 2 or 3 times larger, especially off the main fragment beam. The effect of the (1 − sin) term is to reduce the number of large fragments while leaving the number of smaller fragments ($m << m_{max}$) relatively unaffected. To add to the confusion, Strømsøe and Ingebrigtsen fit data from different regions of the fragment beam separately, with widely different parameters being required for a single warhead.

To examine the relationships between the Mott equation (1), the Held equation (5), and the Strømsøe and Ingebrigtsen equation (8), without supporting fragment data, the following approach was taken.

The Mott equation (1) was taken as the defining relationship. The warhead was chosen to be 10 inches long aand 5 inches in outer diameter, with a 0.25-inch steel wall thickness. Steel density was taken as 7.89 g/cm^3 (129.29 g/in^3). The explosive density was set at 1.6 g/cm^3 with P_{CJ} = 240 kbar. The "maximum" size fragment was defined approximately by setting N(m) = 1 and finding the corresponding value of m_{max} = 62.247 g. In a sense this is equivalent to saying "there is one fragment larger than 62.247 grams and we will ignore it."

The Strømsøe and Ingebrigtsen (SI) equation (8) was solved with μ_o = M and $2\mu_k$ = M_{ave} from the Mott equation (1) and m_{max} = 62.247 g. The Held equation (5) was solved by determining C_H by assuming the singular point m(1) = 62.247 grams and solving for λ after determining the mass of the twentieth fragment from equation (1).

Spreadsheets were used to examine the relationships of N(m) vs. m, M(n) vs. n, and n(m) vs. n by examining individual fragments (calculated) up to n = 20, by fives to n = 30, by tens to n = 100, and by fifties and hundreds up to the smallest calculated fragment. Average masses were assigned to the individual members of fragment groups above n = 20. As shown in figure 1, the three equations converge for higher fragment numbers (lighter fragments); however, for heavier fragments, N(m) follows the order Mott > Held > SI. If fragment number 1 (i.e., n = 1) is taken to be the heaviest fragment, then its mass according to the three distributions is Mott = 62.247 g, Held = 48.78 g, and SI = 37.93 g.

It can be easily seen from equation (5) that $\log_{10}(\ln(M/(M-M(n))))$ is a linear function of C_H and λ. Therefore figure 2a shows this relationship for the calculated Mott and Held distributions (where (~M) = M/(M-M(n))); the slight deviation of the Mott formula from linearity can be seen. The relationship between n and mass is examined in figure 2b, which shows calculated numbers of fragment in different mass ranges for the Mott distribution and for the Held distribution. Two methods were used for calculating the Held distribution: equation (6) (n, Held deriv) and equation (7) (n, Held delta). The distributions are substantially the same except for differences at the very largest fragments.

The Pantax report uses a Mott distribution with a modified Magis equation (no explicit dependence on C/M).[7] For design purposes, a confidence level, CL, is defined as the probability that the mass m_f is the largest mass fragment released. If the Pandex equation (9) is used, all the maximum fragment sizes discussed above are well above the 99% probability level.

$$CL = 1 - \exp(- (m_f/\mu_j)^{1/2}) \quad \text{or} \quad m_f = \mu_j^2 \ln^2 (1 - CL), \text{ for CL} < .9999 \qquad (9)$$

Based on this evaluation, it appears adequate to use a Mott distribution for a priori predictions of fragment size distribution, but to ignore 10 or more (depending on case length) of the largest fragments to assure conservative estimates of target damage.

For noncylindrical portions of warheads typified by the front ends of artillery or bomb warheads, the usual approach is to treat the region of the warhead with decreasing diameter as a set of short cylinders but to ignore any effects of stand-alone short cylindrical warheads discussed subsequently in this paper (equations (22) through (24)).

Fragment Spatial Distribution

The spatial distribution of fragments about a detonating cylindrical warhead is not uniform. Naturally fragmenting metal warhead cylinders typically experience shear fracture initially into F = 20 to 23 initial long axially oriented bands: therefore, the typical band width (peak to peak or valley to valley) about the cylinder axis varies between 15 and 18 degrees. These bands break up further both radially and longitudinally during subsequent expansion into the ultimate fragment size distribution given approximately by the Mott distribution. However, the number of fragments per angle increment may vary by as much as a factor of 4 or 5 between the peaks and valleys caused by the initial fracture. Sewell[8] gives a rule of thumb that the number of initial fracture sites is given by equation (10). Data indicate that end effects produce smaller fragments at both ends of a cylindrical case.

$$F = V_c / (2u_{pc}), \text{ number of fracture sites = number of axial fragment bands.} \qquad (10)$$

where

V_c = initial circumferential velocity of inner wall = 2π(radial velocity).. Radial velocity is approximated by the sweeping wave pressure divided by the wall acoustic impedance. For steel and a typical explosive this radial velocity would about (20-GPa)/(45.2-GPa/mm/μs) = 0.442-mm/μs.

u_{pc} = critical particle velocity. For typical warhead-case steel, u_{pc} for shear is 200 ft/s or 0.061 mm/μs. With these input values, F = 22.8.
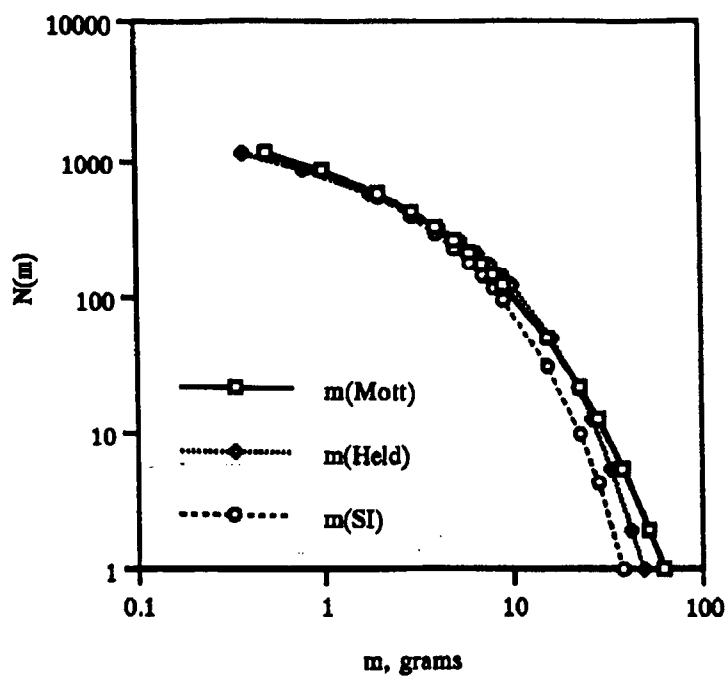
Figure 1. Comparison of Mott, Held, and Strømsøe and Ingebrigtsen (SI) equations for fragmentation, normalized to a common basis.
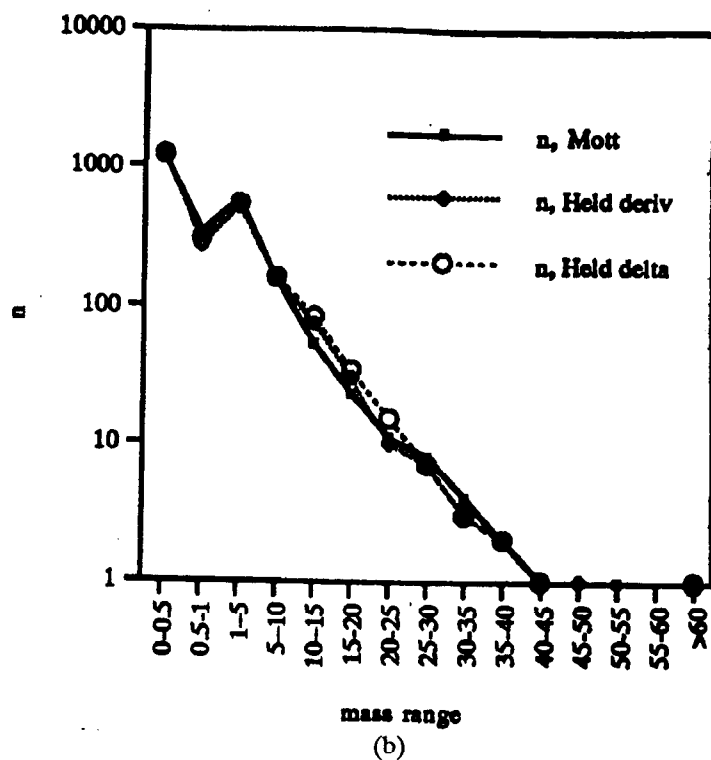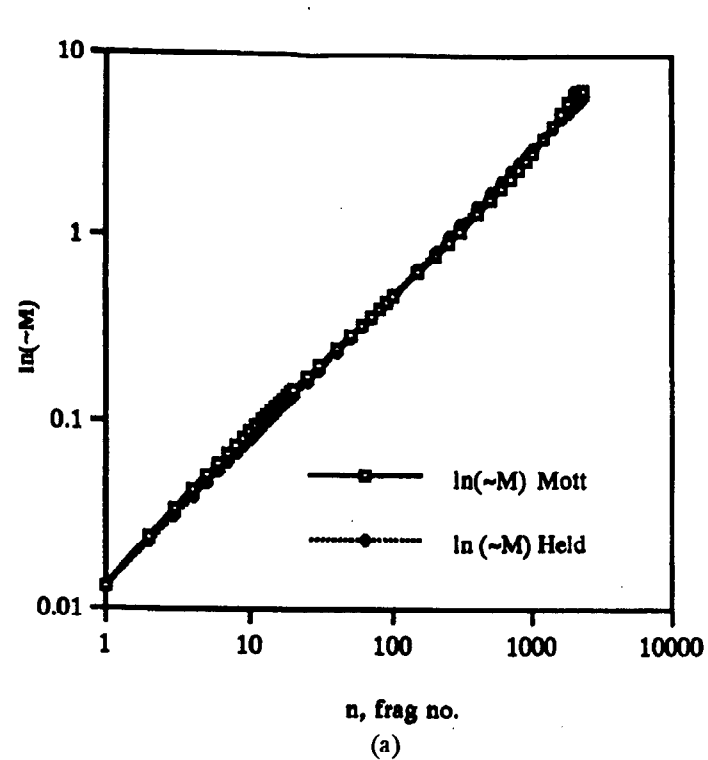

(a)

(b)

Figure 2. Comparison of Mott and Held formulations for (a) ln (~M) = ln[M/(M-M(n))], and (b) number of fragments in individual mass ranges.

The azimuthal (polar) distribution of fragments is limited to a fan with small angular dispersion as shown in Figure 3. For single-end initiation, the peak angular fragment density is angled from the normal (90°) by an amount that can be approximated by one-half the Taylor angle[9], θ, or about 5° given by different authors in both forms shown by equation (11).

$$\tan \theta = (V_o/2D) \text{ or } \sin \theta = (V_o/2D) \tag{11}$$

For portions of the case that are not parallel to the axis of symmetry, the modification of equation (11) given by equation (12) is sometimes used. This can be used to account for fragment velocities from the front ends of typical artillery or bomb warheads, provided the value of C/M is adjusted to account for local variations in cross section.

$$\tan \theta = (V_o/2D) \cos (\pi/2 + \phi_2 - \phi_1) \tag{12}$$

where

ϕ_1 = angle that the normal to the casing at the point makes to the axis of symmetry.

ϕ_2 = angle that the normal to detonation wave front (at the same point on the casing) makes to the axis of symmetry.

V_o = initial fragment velocity, defined below.

None of these equations accounts for end-spray fragments that may occur.

The band or fan of fragments from a cylindrical warhead is not as narrow as equations (11) and (12) imply. Figure 3 shows typical fragment polar-angle (azimuthal) patterns that have been measured for end- and center-initiated warheads in both differential and cumulative plots.

The differential (percent of total fragments per degree) patterns are approximated by equations (13) and (14). The cumulative patterns are obtained by integrating or summing these equations. Here θ is the angle the fragment trajectory makes to the cylinder axis of symmetry.

$$\text{End initiated, } \%/\text{degree} = 11 \exp(- 0.04 (95 - \theta)^2) \tag{13}$$

$$\text{Center initiated, } \%/\text{degree} = 1.1694 \sqrt{(25 - ((90 - \theta)/2.2)^2)} \tag{14}$$
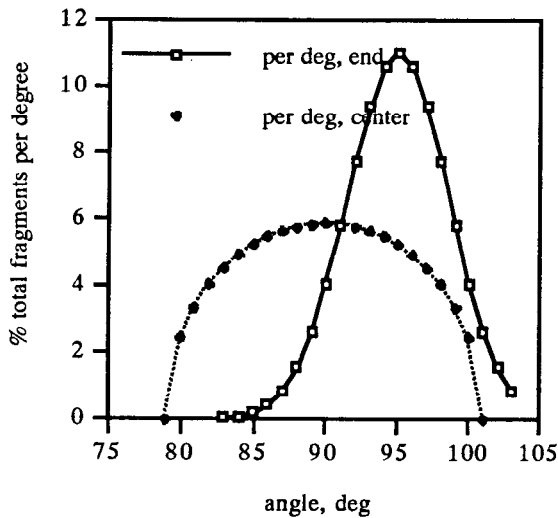

Figure 3a. Azimuthal differential percentage fragment spatial distribution, per degree for end- and center-initiated cylindrical warheads.
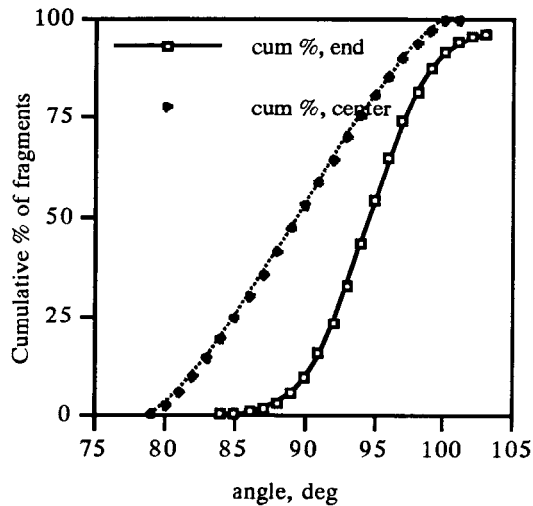
Figure 3b. Azimuthal cumulative percentage fragmet spatial distribution for end- and center-initiated cylindrical warheads.

Fragment Velocity

The "initial velocity" of fragments released in the detonation of a cased explosive is approximated by the Gurney formulas. Actually, the velocity found in this way is the maximum velocity achieved by the fragments during the acceleration phase, and applies to the expanding warhead case fragments only at distances from the warhead center greater than about twice the warhead initial radius. An initial step increase in the case velocity is imparted by passage of the detonation shock wave through the metal. For cylindrical steel warheads, initial elastic-plastic expansion of the case occurs as it expands from the original radius to about 1.2 times the radius. At the end of this phase the case radial velocity is about 60% of the calculated "Gurney velocity." The maximum velocity (95 to 100% of the Gurney velocity) is that achieved at the end of fragment acceleration with the fragments at a radius of about 1.6 to 1.8 times the initial warhead radius. At this time, the detonation products appear in the openings in the fracture and subsequently develop an expanding cloud beyond the fractured warhead case. In the final phase of terminal flight, beyond about 20 times the initial warhead radius, unhindered fragments emerge from the detonation-products cloud (typically reduced in speed by drag to about 90% of the Gurney velocity). Subsequent fragment velocities are subject to deceleration by continuing drag forces in the surrounding medium.

The simplest expression of the Gurney formula for symmetrical configurations is

$$V_{Gurney} = \sqrt{\{2E / (\mu + n/[n + 2])\}} \tag{15}$$

where

μ = M/C, and M= mass of metal in "warhead case" and C= mass of explosive charge.
$\sqrt{2E}$ = "Gurney constant" in units of m/s or ft/s.

Values of n are 1 for a flat sandwich of explosive between two equivalent flat metal plates, 2 for a cylinder, and 3 for a sphere.

In addition, formulas for unsymmetrical sandwiches are useful for flyer-plate warhead-booster performance calculations. Equation (16) may be used for an "open-faced sandwich," with metal on only one face, although other formulas have been proposed as well.

$$V_{Gurney} = \sqrt{\{2E / \{ \mu + ([1+2\mu]^3 + 1)/(6[1 + \mu]) \} \}} \tag{16}$$

For an unsymmetrical sandwich with metal mass of N on one face and M on the other

$$V_M = \sqrt{\{2E /(1 + A^3)/(3 [1+A]) + A^2 N/C + M/C\}} \quad \text{and} \tag{17}$$
$$V_N = A V_M$$

where A = (1 + 2 [M/C]) / (1 + 2 [N/C]).

The Gurney constant, $\sqrt{2E}$, can be approximated by the simple expression:

$$\sqrt{2E} = 0.338 D, km/s \tag{18}$$

where D is the detonation velocity, or by the equation of Kamlet and Finger[10]:

$$\sqrt{2E} = 233 \, \rho_0^{-0.6} \, P_{CJ}^{1/2}, m/s \text{ (with } P_{CJ} \text{ in kbar = 0.1 GPa)} \tag{19}$$

For a cylindrical warhead, the appropriate Gurney formula is applicable only for the cylindrical portion, and the values of M and C used must be adjusted to eliminate end effects. A recent Russian paper[11] published expressions applicable to the ends of cylindrical warheads. Equation (20) is derived from that work.

$$V_{end} = \sqrt{(d M V_{Gurney} /4 L m)} \tag{20}$$

where

d = warhead diameter
M = mass of warhead case cylinder section
L = warhead cylinder length
m = mass of warhead case end section

Data indicate that adjustments must often be made to this simple approach to calculating fragment velocity. Kennedy's survey of fragment velocity data concluded that the Gurney constant (or velocity), as calculated above, is applicable only in the range of 1 < C/M < 2.[12] For C/M of 0.8 or less, Kennedy recommended that the Gurney constant be reduced by a factor of 0.9, while for C/M greater than 2.5, he recommends $\sqrt{2E}$ be increased by a factor of 1.03. Kennedy also noted that fragment velocities from cylindrical warheads with L/D < 1.5 were reduced by a factor related to the L/D value. Equation (21) reproduces Kennedy's curve.

$$V_{actual} = C \cdot V_{Gurney} = (2.32 + .912\,(L/D) - .276\,(L/D)^2) \cdot V_{Gurney} \tag{21}$$

Velocity variations at the ends of cylindrical warheads were reported to be significant by Zulkowski, who obtained the velocity-correction-factor models summarized in equations (22) through (24) by fitting data.[13] These equations are for cylindrical warheads of total length L and explosive diameter d, and actually apply to the speed of the fragments rather than to the velocity vector whose direction must be determined separately.

For single-point initiation at the center of one end

$$C = (1 - e^{-2.3617\,l/d})(1 - 0.28806\,e^{-4.603(L-l)/d}) \tag{22}$$

For center-point initiation

$$C = (1 - 0.28806\,e^{-4.603\,l/d})(1 - 0.28806\,e^{-4.603\,(L-l)/d}) \tag{23}$$

For simultaneous initiation at the centers of both ends

$$C = (1 - e^{-2.3617\,l/d})(1 - e^{-2.3617\,(L-l)/d}) \tag{24}$$

These formulas are not intended to a$\cdots$ y to warheads with appreciable end confinement or with hollow explosive charges. It may be rationalized that these end effects occur because release at the end of the cylinder following face-on impact of the detonation wave prevents the pressure buildup necessary to impart the full Gurney velocity to the side walls.

Velocity of Expanding Warhead Case

The acceleration of an expanding cylindrical warhead case accompanying detonation is approximated by Eq. (25) for cases with wall properties ρ_{oc}, c_{oc}, and s_c.[46]

$$V_R/V_{Gurney} = Max\,(V_o/V_{Gurney}\,,\quad [K(1 - (R_D/R_E)^2)]^{1/2}\,) \quad <1.0 \tag{25}$$

where:

$V_o \sim \{[(c_{oc}^2 + 4\,s_c\,P_c/\rho_{oc})^{1/2} - c_{oc}]/2s_c\}(R_D - t_c)/R_D$,
   the particle velocity in the donor case times a radial expansion factor.

$P_c \sim \rho_{oc}\,P_{cj}\,/(\rho_{oc} + \rho_{oe})$, the approximate pressure induced in the donor case by a grazing detonation wave.

(The pressure in a case of material c due to a normally incident detonation wave is given by $2 \cdot P_c$.)

R_D is the original case radius; t_c is the case wall thickness; R_E is the expanded radius; and K is a constant representing the degree of combustion that occurs during detonation. For explosives that release virtually all their energy in the detonation, the value of K is of the order of 1.35. When the value obtained with equation (25) is greater than unity, V_R should be set equal to V_{Gurney}. P_{cj} is the detonation or Chapman-Jouget pressure of the explosive. This formulation provides some accounting for initial expanding velocity (V_o) of the donor case due to a sweeping detonation wave.

The author has found that logarithmic equations provide even better and more consistent agreement with a wide range of case expansion data. Even data from measurements on case expansion of dual-explosive warheads with major afterburning contributions is fit precisely. Equation (25a) is therefore recommended for values of [(R_E–R_D)/R_D] between about 0.05 and 1.0 or greater, especially for warheads containing explosive compositions that afterburn and therefore continue to accelerate fragments.

$$V_R = Max(V_o,\ A + B\,\log\,[(R_E - R_D)/R_D]\,) < V_{Gurney} \tag{25a}$$
where: $A = 0.321\,x^2 - 0.484\,x + 1.379$
   $B = 0.209\,x^2 - 0.539\,x + 1.100$
   $x = V_{Gurney}\,K^{1/2}$ from equation (25)

Summary of Warhead Fragmentation

The information provided in this section is sufficient to use for predicting fragment size distribution, fragment density patterns, and fragment velocities for axially symmetric warheads against target volumes. Although the method is not completely explicit, enough information is given to calculate results for specific preliminary warhead designs.
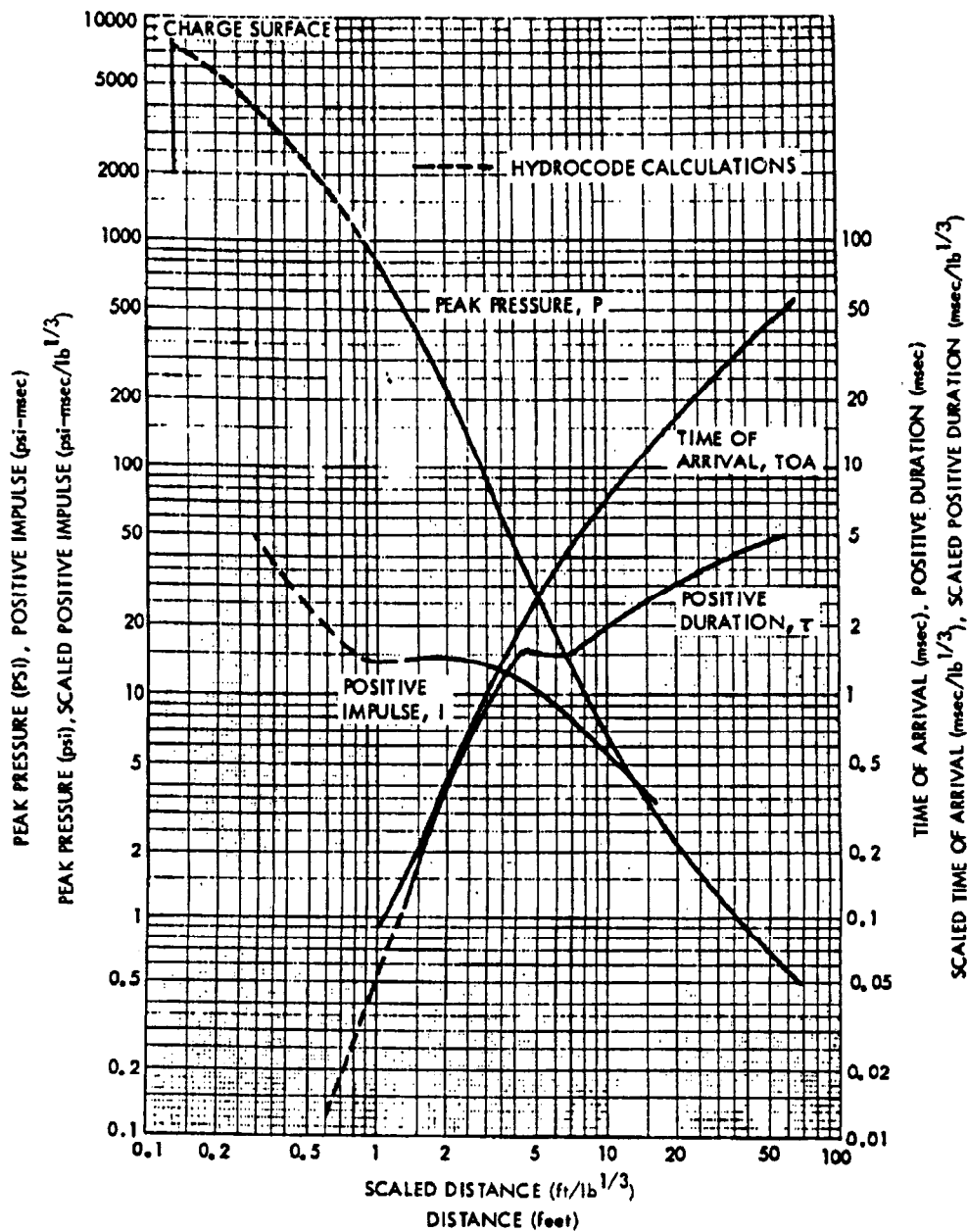
Figure 4. Shockwave parameters for a one pound spherical TNT charge in free air.

WARHEAD BLAST OUTPUT

Spherical Charges

Published standard curves and tables (see figure 4) show the effect of distance from the charge center on the peak overpressure and positive impulse (positive impulse is positive overpressure integrated over time) due to detonation in air of standard spherical masses (1 kg or 1 pound) of bare cast-TNT explosive charges.[14,15] These standard values are scaled to other spherical charge masses by application of the simple scaling laws given later. Different explosives are assigned values of "equivalent weight factor," EWF, which is the ratio of the weight of TNT that will give the same curves to the weight of the explosive of interest. There are also reports of the effects of ground wave reflections, of nonspherical charge shape, and of confining case mass on the measured blast output.[15-21] Corrections for ground reflections, especially for nonspherical charges and for cased charges, are complicated, uncertain, and subject to debate. However, there are substantial data on these effects, even if they do not agree.

Theoretically, a given peak pressure will occur at a distance from an explosion that is proportional to the cube root of the energy yield; this is known as cube-root scaling or Hopkinson scaling, and is known to hold over a very wide range of explosive weights. Because of this, a scaled distance is defined in terms of the actual distance, R, to a specific pressure and the explosive (TNT) weight, W, as $Z = R/(EWF \cdot W)^{1/3}$. Because the standard curves and tables are given for unit weights (1 pound or 1 kilogram) of explosive, the distance values on those curves represent values of scaled distance, as labeled in figure 4.

The peak overpressure and the peak impulse result from shock waves traveling in air. These shock waves are created as the explosive detonation products expand supersonically into the surrounding air. When the pressure at the detonation products/air interface reaches a value such that the shock wave velocity in the air is greater than the velocity of the detonation products, the shock wave is "launched." The shock wave decelerates as its pressure decreases with increasing distance from its source and finally reaches sonic velocity and becomes an ordinary sound wave. While this shock wave can cause damage when it interacts with structures, it is an effective structural destruction mechanism only at fairly small scaled distances (< 20 ft/lb$^{1/3}$). The threshold for eardrum rupture in humans occurs at smaller scaled distance (about 12 ft/lb$^{1/3}$). The blast wave from a large explosion (nuclear scale), however, can cause significant wind effects that may damage structures even after it has become subsonic. When the explosion occurs within a confined space, the major damaging impulse involves the total overpressure integrated over a fairly long time that includes energy contributed by afterburning of incompletely reacted detonation products. Significant internal-blast damage is done by much smaller explosive quantities than are required for external blast damage. The pressure ultimately developed in such internal explosions, subsequent to shock wave propagation and reverberation, is shown later to be proportional to the explosive's heat of combustion.

Figure 4 shows clearly that peak overpressure is a nonvarying function of scaled distance.[15] All the other variables in figure 4 (i.e., positive impulse, I; time of arrival, TOA or t_a; and positive duration, τ (length of time that the initial overpressure pulse is greater than ambient pressure) are scaled quantities that must be multiplied by $(EWF \cdot W)^{1/3}$ to determine their absolute values in a specific situation.

The local shock wave velocity, U, corresponds to a local Mach number $M = U/c_0$, where c_0 is sonic speed in the ambient air. This corresponds to a pressure jump, or local overpressure, $p = P_s - P_0$, where P_s is the local shock-generated pressure and P_0 is the ambient atmospheric pressure.

$$p = P_s - P_0 = 2\gamma (M^2 - 1)/(\gamma + 1) P_0 \ \{ = 7(M^2 - 1) P_0 /6, \ [for \ \gamma = 1.4 \ only] \ \} \qquad (26)$$

The instantaneous velocity of the air-blast shock wave can thus be written as a function of local variables.

$$U = c_0 \ \{(1 + [(\gamma + 1)/2\gamma] \cdot p/P_0\}^{1/2} \qquad (27)$$

The time of arrival, t_a, is obtained by integrating $dr = U \, dt$ from the charge radius to the arrival location, R.[14] Considering the physics of the situation, it would be more accurate to integrate from the "launch point of the air shock wave" instead of from the charge radius, but that leaves no way of accounting for the distance from the charge radius to the launch point.

Arrival times can be measured much more accurately than peak overpressures, even though the true initial time is *fuzzy*. Therefore it is common practice to determine EWF from arrival time measurements rather than from actual pressure measurements. When a pressure gage is oriented side-on to the shockwave velocity, the measure pressure is called *side-on*, *incident*, or *static pressure*, When the gage is oriented normal to the shockwave velocity, it is subject to a peak overpressure two or more times greater than the *incident pressure*. The ratio of reflected pressure to the shock wave pressure varies with the incident overpressure level from 2 at low pressures (less than about 0.1 atmosphere -10^4 Pa or 1.45 psi) to as much as 14 at very high pressures. Equation (28) approximates this effect for $P_s/P_0 < 30$, but fails to generate values of $P_r/P_s > 8$.

$$P_r/P_s = 2 + 6P_s/P_0/(P_s/P_0 + 7) \qquad (28)$$

The dynamic pressure, $q = \rho V^2/2 = \gamma PM^2/2$, is essentially the wind loading on the target and is not accounted for in static pressure measurements. For supersonic compressible flow, the solution of dynamic pressure is not trivial. While dynamic pressure has relevence to damage from very large explosions, it is not important for more transient tactical ordnance blasts.

Unfortunately, it is virtually impossible to measure blast parameters in free air at appreciable distances from the charge; this would require that the entire experiment and all gages be sufficiently far from the ground to avoid reflections. One common practice is to mount the charge and the gages sufficiently close to the ground that they are below the triple point at all distances so that all measurements are made in the regime where the shock

waves reflected from the ground have combined with the air shocks. (For spherical charges, the triple point is formed at the intersection on the ground of the incident and reflected waves approximately 40° off the vertical axis from the ground to the charge center.) It is then assumed that the energy incident on the gages is that due to concentrating all the energy into a hemisphere instead of a sphere, and the ratio of apparent yield to actual yield is assumed to be 2.00. This assumption ignores energy losses due to crater formation and ground-yield phenomena. In some approaches, these losses are accounted for approximately by assuming an apparent yield ratio multiplier of 1.50. Other values for the multiplier have also been suggested; the Pantex[7] report suggests using 1.8 if there is cratering; the *Joint Munitions Effectiveness Manual*`(JMEM)[22] suggests using 1.65. The difference due to this uncertainty amounts to only 12 % in the value of Z.

Nonspherical Charges

For nonspherical charges, there are time and directional/orientation effects that may cause yield multipliers to be greater than 2.00. We shall not dwell on this, but consider the following differences between tests on spherical and cylindrical charges. Typically, a spherical charge is center-initiated; the detonation reaches all points on the charge surface simultaneously, and shortly thereafter a spherical air shock wave is launched. Whether a cylindrical charge is initiated at one end, both ends, or at the center, the sweeping detonation wave will cause the air shock to be nonspherical and to develop in a volume surrounding the charge over a time lasting up to several hundred microseconds. There will also be end effects.

Major contributions to the database on cylindrical charge blast output include both vertical[19] and horizontal axis orientations.[20,7] The JMEM provides analytical methods for relating cylindrical and spherical charge output that are recommended here for initial modeling attempts. The recommended JMEM peak pressure equation for cylinders measured normal to the charge axis is

$$P_{cylinder}/P_{sphere} = 5.53 \cdot (L/D)^{0.308} /Z^{0.998} + (Z - L/D)/24.99 \tag{29}$$

where Z = scaled distance.

Further refinements can be obtained by examining Swisdak's[19] results, also for nearly normal orientation, or Plooster's[20,7] results for other orientations.

Cased Charges

Baker[16] compares blast and impulse data from cased bombs and bare spherical charges. Since Baker was also active in the Pantex[7] and JMEM[22] work, one can be reasonably sure that previous investigators have tied much of the existing database together. Held[21] shows curves of six of the models that have been used for case effects on EWF (although Held's figure 9 shows the curves, they are not identified). One of the more commonly used curves for steel casings is the Modified Fano curve, equation (30).

$$W_e/W = .6 + .4/(1 + 2(M/C)) \tag{30}$$

where W_e/W = ratio of effective explosive weight to actual explosive weight. We have found that it is possible to work separately with shape factors using equation (29) or refinements thereto and case factors using equation (30) or its variants to account for relationships between different explosives, different shapes, and different sizes. The pressure multiplier due to ground reflection often remains a questionable variable in considering such data. Overpressure data from detonating cased explosive charges will often show spurious peaks due to shock waves from the passage of supersonic fragments.

For thin cases or case materials more brittle than steel, there are data that show increased blast pressure with cased explosives compared with bare explosives.[7] This is particularly true for cases in which the metal is in particle form bonded in a plastic matrix. Reasons for this effect are the subject of speculation. Filler has demonstrated significant increases in blast overpressure through the use of cases fabricated from reactive metals.[34] This contrasts with Filler's work on spherical inert cases that consistently showed reduced overpressure.[35]

Summary of Warhead Blast Output

The information provided in this section is sufficient to use for predicting the blast output of spherical or cylindrical warheads. Enough information is given to generate results for specific preliminary warhead designs and to vary the results in accordance with variations suggested by the different approaches in the references.

WARHEAD DAMAGE MECHANISMS

Fragment Damage

Fragment damage to targets generally occurs by perforation of the target and deposition of residual energy therein. The THOR equations provide a simple method for preliminary calculations of the limiting velocity, V_o, for perforation of specific target materials of specific thickness as well as the residual velocity, V_r, following perforation, and the residual mass, m_r, of the perforating fragment. All these are calculated for steel fragments as a function of the mass m_s, velocity, V_s, and obliquity to the target surface, θ, of the impacting fragment. The THOR equations do not generate secondary fragments from spalling or fracture of target materials. The general form of the THOR equations is as follows:

$$V_r = V_s - 10^{c_1} \cdot (t_o A)^{\alpha_1} \ m_s^{\beta_1} \ (\sec \theta)^{\gamma_1} \cdot V_s^{\lambda_1} \tag{31}$$

$$m_r = m_s - 10^{c_2} - (t_o A)^{\alpha_2} \ m_s^{\beta_2} \ (\sec \theta)^{\gamma_2} \cdot V_s^{\lambda_2} \tag{32}$$

where

t_o = case thickness, cm
masses are in grams
velocities are in m/s
subscripted parameters (c, α, β, γ, and λ) are characteristics of target materials

A = presented area of fragment at impact in cm^2 = $K m_s^{2/3}$. K = 0.3079 for spherical fragments, K =0.3799 for cubic fragments, and K = 0.5199 for random fragment shapes can be used in lieu of more specific data.

The limiting velocity for perforation is given by equation (33); θ_{max} (equation (34)) is the maximum obliquity angle that will give the desired residual velocity V_{rd}.

$$V_o = \{10^{c_1} \cdot (t_o A)^{\alpha_1} \ m_s^{\beta_1} \ (\sec \theta)^{\gamma_1}\}^{1/(1-\gamma_1)} \tag{33}$$

$$\theta_{max} = \sec^{-1} \{([(V_s - V_{rd})/(10^{c_1} \cdot (t_o A)^{\alpha_1} \ m_s^{\beta_1} \ V_s^{\lambda_1})]^{1/\gamma_1} \tag{34}$$

Figure 5 shows results of spreadsheet calculations using equations (31) through (34). The calculations are for a 16-gram fragment of "random" shape impacting a 1/4-inch-thick target sheet of hard homogeneous steel at 2000 m/s. Following perforation of the sheet, the target thickness that will prevent perforation by the residual mass and residual velocity is calculated. Also shown are values of the ten subscripted parameters for five typical target materials.

The effects of very high velocity fragments on munitions can be calculated with methods presented elsewhere,[23] which account for shock initiation of detonation as well as ignition by perforating fragments (whose residual velocity is determined as above). For shorter distances between munitions, such that the donor case has not completely fragmented when its case impacts a neighboring munition, a method for predicting sympathetic detonation is also available.[24]

Blast Damage

Blast causes damage by imparting motion to a target. This motion may hurl an object that is not fastened down, such as a truck, airplane, or a person; it may activate natural vibration modes to destructive amplitudes, as occurs with buildings; or it may tear parts of a structure, such as a skin stretched between rigid support members. Much has been published on the subject of damage due to blast; after all, this is one of the design goals of ordnance.[7,21,25-30] The behavior of air blasts, as described previously, is relatively straightforward. In contrast, the response of targets to airblast is complicated because it involves the dynamic response of the targets. This is a major specialized discipline of structural analysis within mechanical, aerospace, civil, and architectural engineering fields beyond the scope of this overview. According to Held, "In addition, the interaction between the blast wave is affected by a great number of factors that can either not be determined precisely or are not known at all." [21]

An error frequently made in predicting or assessing blast damage is to correlate the damage to the peak overpressure alone. Peak pressure alone is responsible for damage only if the positive phase duration, τ, is relatively long compared to the natural vibration period of the target structure. Generally this is the case when the target is very soft or when the charge is very large and distant from the target, as for nuclear weapons. Impulse plays the major damage role when the natural vibration period of the target is much longer (approximately four or more times greater) than the positive phase duration.

Kinney and Graham's Table XV[14] gives a correlation for blast damage from large explosions to a wide range of targets as a function of side-on pressure, reproduced here as Table 1. But the user is cautioned to avoid the implication that the magnitude of the peak pressure pressure alone is the causative parameter for all explosions.

An iso-damage hyperbola has been defined by equation (35), wherein DN is a damage number (representing a constant damage curve), and p_c and I_c are constants for a particular target that represent critical pressure and critical impulse asymptotes, respectively.[21,30]

$$DN = (p - p_c)(I - I_c) \qquad (35)$$

Westine[31] developed equation (36) for damage distance, R, that covers all the bases quite well: (1) pressure loading alone (B = C = 0), (2) positive impulse loading alone (B = 0), and (3) iso-damage (combined pressure and impulse loading, C = 0). The constants in equation (36) can be obtained from measurements taken over a wide range of distance and charge weight.

$$R = A\, W^{1/3}/(1 + B^6/W + C^6/W^2)^{1/6} \qquad (36)$$

In a study of damage due to distributed charges (for example, fuel-air explosives), Sewell and Kinney[25,14] proposed a somewhat different approach that nevertheless contains the same physical principles as the iso-damage model. They proposed that to do damage, an explosion must deliver an effective sustained pressure effect for some minimum time. This requires definition of both a critical impulse and a critical time over which it must be applied for damage to a specific target. To maximize momentum transfer to the target, the critical time is no greater than one-quarter of the natural vibration period of the target structure subject to damage, or $t_{cr} = T/4$. Structural damage inflicted by explosive blast is the result of an impulsive load that exceeds the resistance of a material, which, in many cases, can be defined by a critical impulsive load, I_{cr}.[32]

Natural vibration frequencies of various mechanical configurations have been published. Young's Table 36 is a useful, widely available source of such data.[33] For the specific case of a structure with a metal skin fastened to and stretched between two rigid stringers, the natural frequency can be obtained from equation 15.a of Young's table as adapted in equation (37).

$$f = 18.56 \cdot (22.4/(2\,\pi)) \cdot (t_0/a^2)\, \sqrt{(E\, g/12\, \rho\, (1 - v^2))} \qquad (37)$$

where

t_0 = skin thickness, inch

a = separation between stringers, inches

E = modulus of elasticity of skin material, psi ($\sim 11 \times 10^6$ for Al, $\sim 29 \times 10^6$ for steel)

g = gravitational constant, 32.2 ft/s^2

ρ = specific gravity of skin material, g/cm^3 (2.79 for Al, 7.89 for steel)

v = Poisson's ratio for skin material, about 0.3 for most structural metals

The constant 18.56 comprises conversion factors to allow use of the common, mixed units defined above. The constant 22.4 is determined by the problem geometry; for example, for a square grid with the same separation between supports, the constant would be 36.0, and for a rectangular grid with the longer separation equal to 2·a, the constant would be 24.75. For aluminum panel 1/16 inch thick and spar separation of 8 inches, $E = 11 \times 10^6$ psi, and $\rho = 2.79$, equation (37) gives a natural frequency of 212 Hz. This corresponds to a period of 4.7 ms and a critical time, $t_{cr} = 1.2$ ms. For steel sheet, the natural frequency would be about 2% lower.

The critical impulsive load, I_{cr}, can be calculated by any of the three ways shown in equation (38), with typical values for aluminum alloy shown below.

$$I_{cr} = \rho\, t_0 V_c = t_0\, \sigma_y/c_0 = t_0\, \sigma_y(\rho\, /E)^{1/2} \qquad (38)$$

where

V_c = critical particle velocity for failure (240 ft/s for Al)

σ_y = dynamic yield strength (140,000 psi for Al)

c_0 = sonic velocity in the material (16,470 ft/s for Al)

Using these values, $I_{cr} = 45$ psi-ms for the aluminum sheet discussed earlier. Rinehart and Pearson give values of V_c for several metals; the values lie in the range 50-500 ft/s, with 200-250 ft/s being typical except for the harder stainless steels that have values near 500 ft/s.[32] It should be noted that the dynamic yield strength is appreciably greater than conventional static values.

THOR Fragment Penetration Spreadsheet

Material	Residual velocity equation constants					Residual mass equation constants				
	c1	a1	b1	g1	l1	c2	a2	b2	g2	l2
Mild steel	3.69	0.889	-0.945	1.262	0.019	-2.478	0.138	0.835	0.143	0.761
hard homo ste	3.766	0.889	-0.945	1.262	0.019	-2.671	0.346	0.629	0.327	0.88
face-hard st	2.305	0.674	-0.791	0.989	0.434	-1.534	0.234	0.744	0.469	0.483
Cast iron	2.079	1.042	-1.051	1.028	0.523	-8.89	0.162	0.673	2.091	2.71
2024T-3 Al	3.936	1.029	-1.072	1.251	-0.139	-6.322	0.227	0.694	-0.361	1.901

Layer 1

Vs, m/s	2000			Assume random fragment (A=K*ms^.667), K random =0.5199					
ms, g =	16	A=	3.3012	sq cm		Other fragments:	K cube=	0.3799	
targ thick,cm=	0.635						K sphere=	0.3079	
obliq, ang, deg	0								

TARGET MATERIAL: Hard homogeneous steel (row 5)

Residual vel=	1052	m/s
Residual mass	3.341	grams
limit velocity	934.1	m/s for perforation
max obl	56.91	deg for perforation

Layer 2

targ thick,cm=	0.389	A= 1.1616 sq cm
obliq, ang, deg	0	
Residual vel=	0.014	m/s
Residual mass	1.761	grams

Figure 5. Spreadsheet results for THOR penetration equations: 16-gram random-shape steel fragment, 1/4-inch thick, 2,000 m/s impact velocity, hard homogeneous steel target.

Table 1. Blast Damage – Side-on Overpressure Correlation (Large Explosion).[14]

Type of damage	Overpressure, millibars
Minimum damage to glass panels	1 – 3
Typical window glass breakage	10 – 15
Overpressure at limit for debris and missile damage	15 – 25
Windows shattered, plaster cracked, minor damage to some buildings	35 – 75
Personnel knocked down	70 – 100
Panels of sheet metal buckled	75 – 125
Failure of wooded or asbestos panels for conventional homes	75 – 150
Failure of walls constructed of concrete blocks or cinder blocks	125 – 200
Self-framing paneled buildings collapse	200 – 300
Oil storage tanks ruptured	200 – 300
Utility poles broken off	300 – 500
Serious damage to buildings with structural steel framework	300 – 500
Eardrum rupture	350 – 1000
Reinforced concrete structures severely damaged	400 – 600
Railroad cars overturned	400 – 600
Probable total destruction of most buildings	700 – 800
Lung damage	2000 – 5000
Lethality	7000 – 15000
Crater formation in average soil	20000 – 30000

The dimensions used in the example above are typical of an aircraft skin, which we would therefore expect to fail under an impulsive load of 45 psi-ms with a duration of 1.2 ms. The computed minimum blast overpressure for this damage becomes 45/1.2 = 37.5 psi, which must last 1.2 ms to provide the necessary minimum impulse. From the information provided earlier in this paper on overpressure, impulse, and positive duration, τ, the scaled distance at which the necessary impulse will be delivered can be determined. For example, a peak pressure of 75 psi and a positive duration of 1.2 would give an average overpressure (assuming a triangular pressure pulse of duration τ = 2 I/p) exceeding 37.5 over the required time duration at a scaled distance of 3.5 ft/lb$^{1/3}$. This overpressure corresponds to the overpressure from detonation of 1 pound of TNT at a distance of 3.5 feet, or of 100 pounds at a distance of 16 feet; however, the larger charge will have a longer positive duration. If an exponential decay of peak pressure is assumed, an initial peak pressure of about 100 psi is required to give a total positive impulse of 45 psi-ms with a one-pound TNT charge.

This method also gives useful results for calculating damage to light, sheet-metal-covered industrial buildings with approximate values of t_{cr} = 9 ms and I_{cr} = 30 psi-ms. Several other calculated target destruction values using this criterion are: truck (crushing hood or cab) t_{cr} = 1 ms and I_{cr} = 110 psi-ms, armored personnel carrier (crushing roof) t_{cr} = 4 ms and I_{cr} = 800 psi-ms, military tank (crushing thin section) t_{cr} = 2 ms and I_{cr} = 1,600 psi-ms.

For more severe structural damage, for example aircraft wing or empennage breakoff, the same approach can be used. Because of complex monocoque construction, the elastic modulus of such structure requires either finite element solution or measured values. The first mode resonant frequency of such structures on small (fighter or attack) aircraft is known to be about 5 hz, which leads to critical time, t_{cr} = 200/4 = 50 ms. Ignoring support members, the major resistance to failure can be assumed to be that of two skin sections, just twice the value calculated for skin damage, so I_{cr} = 90 psi-ms.

For human fatality, the estimated criteria are t_{cr} = 3 ms and I_{cr} = 290 psi-ms.

For objects that are not fastened down, such as trucks, aircraft, or personnel, Sewell and Kinney relate damage to the ability of the blast wave to hurl the object. It is assumed that serious damage is done on impact when the hurled object is stopped. The criterion for hurling was arbitrarily chosen as the impulse required to achieve free-fall velocity (32.2 ft/s) in 1 second, or I_{cr} = W·t/A. With this assumption, for a 15,000-pound aircraft with a side-on area of 200 ft^2, I_{cr} = 520 psi-ms. Other I_{cr} values calculated by this method are 400 psi-ms for a truck, 500 psi-ms for an armored personnel carrier, and 5,000 psi-ms for a military tank.

While the distance to constant blast overpressure is expressed as $R = k\,W^{1/3}$, the damage effects observed above are roughly expressed in terms of higher powers of W, ranging from $W^{1/2}$ for energy flux to $W^{0.55}$ for reflected impulse and $W^{2/3}$ for side-on impulse. Therefore, the blast-damage radius for a given weight of explosive drops off more slowly than would be calculated on the basis of overpressure alone.

Summary of Warhead Damage Mechanisms

This section has presented analytical methods that can be used to estimate damage from warhead fragments or blast to a number of types of targets. Information needed to extend the range of target types and structural configurations is available in the cited references.

INTERNAL BLAST

Internal blast is treated here as a separate category from the external blast effects and damage discussed earlier. Internal blast effects concern the overpressure, positive impulse, and damage effects of rapid energy release within unvented and partially vented enclosures. The phenomena responsible include energy release from detonations of explosive materials as well as explosions of gaseous fuels and dusts. In this paper we are concerned only with detonations of explosive materials. This is particularly relevent for such phenomena as bombs and artillery shells detonating inside buildings or vehicles and HEI cannon rounds detonating within aircraft bodies. The open literature contains enough information on this subject for one to be certain that much more is contained in restricted publications.[7,14,29,36-40] From experimental measurements of incident pressure in confined spheres, tubes, and cubes, Weibull[36] found that equation (39) fit all the incident overpressure data quite well for 0.003 < W/V < 0.2.

$$p = 166\,(W/V)^{0.72} \tag{39}$$

where

p = overpressure in bars (1 bar = 14.5 psi)
W = TNT weight in pounds
V = compartment volume in ft^3

Although it is not noted in the literature, equation (38) is almost identically the incident pressure, given by figure 4 over the range $0.0001 < W/V < 0.2$ (i.e., $1 < Z < 10$), such that equation (40) for scaled distance ($Z = R/W^{1/3}$) is a perfect fit for spherical volumes of radius R.

$$Z = [(4\pi/3)(W/V)]^{-1/3} \qquad (40)$$

Kinney, et al.[37] demonstrated the effect measured by Weibull with thermodynamic calculations. Thus, it would appear that the peak incident overpressure in internal blast is virtually the same as that measured in free air, and will therefore be unaffected by venting of the chamber.

Baker, et al.[7] describe reverberation of the shockwave in internal blast. The pressure amplitudes of the successive reverberations are lower than the initial shockwave as 1:1/2:1/4: etc. Baker states that to a first approximation, for structures having a low resonant frequency, the effect of internal blast can therefore be approximated by a wave that considers only the initial pulse and the first two reverberations, and can be approximated by 1.75 times the pressure (and equally the impulse) of the free-air values. The duration time from arrival of the initial pulse to decay of the nth pulse is (ignoring reduced velocity of subsequent weaker shock waves as well as higher sonic velocity as more gas in the chamber is heated by mixing with combustion products) approximately $(2n-1)t_a + \tau$. Oscilloscope traces published by Weibull show duration time from arrival of the initial pulse to the end of exponential decay in his chamber of the order of 5 seconds.

A correlation can be drawn between an explosive's heat of combustion, heat of detonation, and its EWF. The method of Baroody and Peters[41] was used to calculate explosive heats of detonation using NWC's PEP (Propellant Evaluation Program) Code.[42] The PEP Code's option 8 was used to calculate heat of combustion ($Enthalpy_{Tc,1\ atm} - Enthalpy_{298K,1\ atm}$). TNT is a rather unique explosive; it, as well as DNB and DNT, is underoxidized so that its equilibrium state, following detonation, has a significant quantity of unreacted compounds (CO, H_2, and particulate carbon). Other explosives such as RDX and HMX are balanced or overoxidized and thus have lower fuel species concentration in their calculated equilibrium states following detonation. It is also likely true that none of these explosives is in its equilibrium state following the very rapid combustion process of detonation, but equilibrium thermodynamics cannot handle this problem. To compensate, thermodynamic properties of explosives are often calculated assuming varying degrees of reaction completeness. Kinney's calculation indicates that within the zone between $Z= 0.4$ and $Z = 2.1$, an excellent fit to Weibull's data is obtained if the final products of the TNT reaction are allowed to progress through the nonequilibrium final states of $CO-H_2$, $CO-H_2O$, CO_2-H_2, to the equilibrium CO_2-H_2O state. For lower values of Z (or higher values of W/V, as Kinney applied them), carbon particles form in the reaction.

Most EWF data obtained from air-blast tests can be rationalized to a combination of an explosive's heat of combustion and heat of detonation ratioed to the heat of combustion of TNT, as defined by equation (41) and shown in Table 2 for several common explosives.

$$EWF = a\ \Delta H_{comb,x}/\Delta H_{comb,TNT} + (1-a)\Delta H_{det,x}/\Delta H_{comb,TNT} \qquad (41)$$

Of the explosives in Table 2, only HMX (and TNT by definition) appears to be completely combusted prior to launching the air blast wave. If complete combustion of the explosive and any oxygen-poor detonation products occurs early enough to drive the air-shock wave, one would expect to obtain EWF values given in the third column of Table 2. The additional energy available in an interior blast, when compared to free-air values, would come from the difference between the values in the second and third columns of Table 2.

The method of Baroody and Peters can also be used to calculate the energy available from reactive cases or liners. This can add greatly to the available heat of combustion if the reactive materials are finely divided or the available reaction time is sufficiently long. In external blast scenarios, the role of reactive aluminum, magnesium, or titanium is more incendiary.

The initial internal blast loading parameters are, in most cases, the normally reflected parameters. Therefore, the reflected overpressure, as determined by equation (27), should be used to determine damage effects as described earlier. It seems likely that the initial peak pressure will be related to the EWF as determined in free air tests (second column of Table 2), but that subsequent pressure peaks may be amplified above the values suggested by Baker[7] by subsequent reaction of detonation products. Therefore, for the explosive AFX-931, the multiplier of

1.75 suggested by Baker may well become as high as 1.92. Considerably higher multipliers may be achieved with reactive-case or reactive-liner warheads.

Table 2. Relationship Between Measured EWF and ΔH_{comb} and ΔH_{det}.

Explosive	EWF data	$\dfrac{\Delta H_{comb,x}}{\Delta H_{comb,TNT}}$*	$\dfrac{\Delta H_{det,x})}{\Delta H_{comb,TNT}}$	a
TNT	1.0	1.0	0.81	1.0
RDX	1.11	1.136	1.07	0.61
HMX	1.15	1.13	1.07	----
H-6	1.38	1.49	1.22	0.59
PBXN-107	1.41	1.45	0.925	0.924
PBXN-109	1.34	1.44	1.19	0.6
AFX-931	1.16	1.43	1.08	0.23

*$\Delta H_{comb,TNT}$ = 1423.7 cal/gram (calculated)[41]

The duration of elevated pressure following a confined explosion will depend on several factors. In a completely enclosed volume that retains integrity following the explosion, only slow cooling of the confined product gases will cause a pressure drop. For example, a 100-pound TNT charge reacting completely to gaseous products in a 10,000-cubic-foot enclosure, originally at standard atmospheric pressure and 298 K, will result in a final, cooled overpressure of about 0.19 atmospheres. It combustion of air is considered, the average (quasi-static) overpressure of the heated gas due to the combustion is about 3.2 atmospheres after shock reverberations have damped. (The peak incident overpressure for this geometry, calculated with equation (38), is about 6.0 atmospheres.) The ratios of these three values are not general, but are specific to this geometry. For example, for an enclosure with ten times the volume, the peak incident overpressure will be about 1.13 atmospheres, the final, cooled overpressure, about 0.019 atmosphere, and the average hot overpressure, about 0.36 atmosphere. All these calculations ignore entropy losses in the shock processes.

An enclosure may be vented, either by its construction, by damage caused by entry of the warhead, or by blowout of frangible panels, to prevent total destruction. Finally, the entire structure may be "blown out" or demolished by the blast. A structure demolished by a detonation within can be a very hazardous source of secondary fragments. It is desirable to vent the structure to reduce this kind of hazard even though the enclosure and its contents cannot be protected from the initial blast shock wave.

Pressure decay for vented enclosures has been modeled in terms of scaled quantities as shown in equations (42) through (44).[43,7]

$$t = 0.4695\,(V/A_v\,c_o)\,\ln\,((p + P_o)/P_o), \quad \text{time to vent enclosure} \tag{42}$$

$$i_g = (P_o V/A_v\,c_o)\,[0.4695(e^{2.13\,\tau'} - 1) - \tau'\,], \quad \text{total gas impulse in chamber} \tag{43}$$

$$p(t) = p\,e^{-2.13\,\tau'}, \quad \text{pressure in chamber as a function of time} \tag{44}$$

where

$\tau' = t\,A_v c_o/V$ = scaled time

p = overpressure in same units as P_o (ambient or final pressure after venting)

A_v = vent area (for single-walled structure) in same units as volume (V)

c_o = sonic velocity in air (340 m/s) in same units as V

When solving equations (42) and (44), Baker sets the initial pressure to the peak incident overpressure, p, the value obtained using equation (39). This is just a rationalized approximation. The peak pressure at the enclosure wall is the reflected pressure. Repeated reverberations will initially cause a series of lower-amplitude shocks to impinge on the wall. During the time of these shock reverberations, afterburning combustion of detonation products will continue and the "quasi-static" pressure at the wall will be increasing due to mixing of hot detonation products and other combustion products with the unreacted air in the chamber. Some degree of equilibration is reached; however, according to this model, during this entire time the pressure in the chamber is dropping as given by

equation (44). If a 100-pound TNT charge detonated inside a 10,000-cubic-foot chamber with a 10-square-foot vent area (0.45% of the enclosed spherical surface area), equations (42) and (43) give the venting time, t = 816 ms and the total gas impulse, i_g = 24,800 psi-ms. For an enclosure of this size, a larger vent is required to cause a faster pressure drop and a substantial reduction of total gas impulse. For example, a 100-ft^2 vent will give t = 81 ms and i_g = 2,460 psi-ms. This estimate may be conservative from the viewpoint of designing a vent size. In an earlier paragraph, the sustained or peak quasi-static overpressure in this situation was estimated to be 3.2 atmospheres (following damping of reverberations). Equation (42) can be used to calculate the time from the initial incident pressure peak (6 atm = 87.3 psi to the estimated average overpressure of the heated gas due to the combustion (3.2 atm = 47 psi) as 26 ms. This is to be compared with Baker's (nearly identical for this case) estimated duration time of the transient reverberation phase, $(2n-1)t_a + \tau$ = 24.6 ms (for n = 3), as given earlier. It is a more difficult problem to estimate the growth time of the quasi-static pressure as a function of position in the enclosure, since it involves a combination of combustion rates, detonation product particle velocities, and turbulent mixing. These concepts are illustrated by figure 6 for the enclosure with a 100 ft^2 vent, assuming the growth of the quasi-static pressure to occur linearly at sonic velocity. It appears that the differences between the results using the simplified method based on peak incident pressure and the method combining reflected pressures and quasi-static pressure are not too great. A more complete solution is beyond the scope of this paper.

Essentially two mechanisms participate when explosives are detonated within confined structures. The first is a transient effect due to the impulse to the walls upon reflection of the blast shock waves. The second mechanism is due to a much greater sustained ("quasi-static") pressure rise caused by additional gas from detonation and combustion of the explosive and the temperature rise of all gas in the enclosure. The time duration and impulse transfered to the enclosure walls by this second mechanism can be reduced by designing the enclosure with appropriately sized vents.
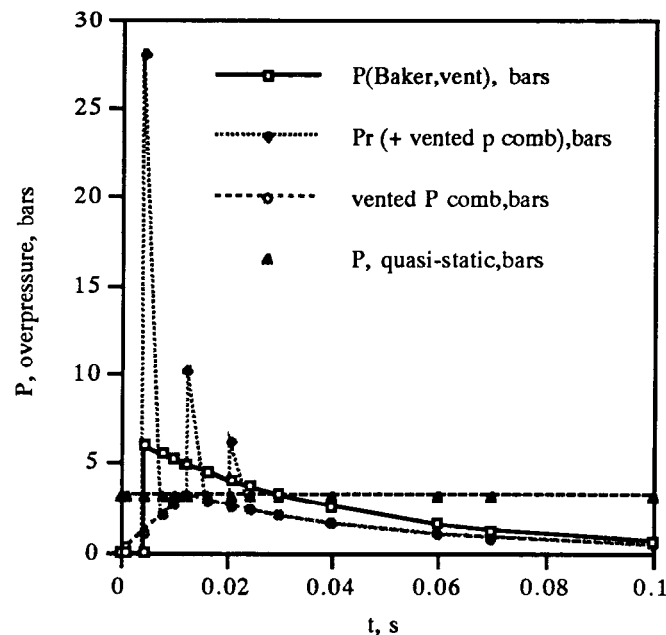

Figure 6. Time history of pressure in 10,000-ft^3 enclosure with 100-ft^2 vent following detonation of 100-lb TNT. Dotted line represents Pr, reflected pressure at the wall, referenced to the rising quasi-static pressure due to equilibration of internal gas heating. Horizontal line represents quasi-static pressure without cooling or venting. P(Baker, vent) represents equation (43) as applied by Baker to the calculated peak incident pressure, 6 bars, as described in text; vented p comb represents applying equation (43) to the calculated quasi-static pressure, 3.2 bars, assuming initial linear growth of the pressure at the wall occuring at sonic ambient-air velocity.

BLAST FROM NONDETONATING EXPLOSIONS

In hazard scenarios we are concerned about overpressures generated when ordnance explodes or "deflagrates" as the result of combustion of enclosed energetic material. Shock wave pressures can be generated when vessels are burst by internal gas overpressure. Kinney's method generates values for energy of explosion from the internal pressure and volume of the bursting vessel.[14] These values of energy are related to the energy in TNT explosive to obtain an equivalent weight of detonating TNT. Baker's more complicated method gives values of burst energy that are the same as Kinney's at high vessel pressures (> 4000 psia) but slightly lower at lower pressures.[16] Kinney's method, as given by equation (45) is more widely used, reportedly with success for both gas-filled pressure-bottle bursts and explosions due to combustion of energetic material contained in a vessel. Equation (45) ignores the effects of energy transfer to debris. The effects of afterburning subsequent to burst would be calculated by the method of the previous section.

$$E = [PV/(k-1)] \, [1 - (P_a/P)^{(k-1)/k}] \tag{45}$$

$EW = E/(4.610 \times 10^6)$, explosive yield in TNT equivalents, kg; with E in joules.

where

E = energy of explosion in consistent units
V = volume of the exploding vessel at absolute pressure, P
P_a = ambient pressure into which the gas expands
k = heat capacity ratio for the gas

REFERENCES

1. Pearson, J., *A Fragmentation Model Applied to Shear-Control Warheads*, Naval Weapons Center, China Lake, California, NWC TP 7146, May 1991.

2. Held, M. and Kühl, P., "Consideration to the Mass Distribution of Fragments by Natural-Fragmentation in Combination with Preformed Fragments," *Propellants and Explosives*, 1, pp. 20-23, 1976.

3. Mott, N.F., *Fragmentation of H.E. Shells: A Theoretical Formula for the Distribution of Weights of Fragments*, A.O.R.G. Memorandum 24, also NOS-AC-3642, 1943.

4. Magis, S.F., *Material Selection for Naturally Fragmenting Munitions*, NWL TM 13/67, 1967.

5. Held, M., "Fragment Mass Distribution of HE Projectiles," *Propellants, Explosives,, Pyrotechnics*, 15, pp. 254-260, 1990.

6. Strømsøe, E. and Ingebrigtsen, K.O., "A Modification of the Mott Formula for Prediction of the Fragment Size Distribution," *Propellants, Explosives, Pyrotechnics*, 12, pp. 175-178, 1987.

7. US Department of Energy, *A Manual for the Prediction of Blast and Fragment Loadings on Structures*, DOE, Pantex Plant, Amarillo, Texas, DOE/TIC-11268, November 1980. Much of the information in this report is included in the book *Explosion Hazards and Evaluation*, by W.E. Baker, et al., Elsevier, New York, 1983.

8. Sewell, R.G.S., *Fragmentation of Uncontrolled Cylinders*, COMARCO, Ridgecrest, California, Sept 1987.

9. Walters, W.P. and Zukas, J.A., *Fundamentals of Shaped Charges*, John Wlley and Sons, New York, 1989.

10. Kamlet, M. and Finger, M., "An Alternate Method for Calculating Gurney Velocities," *Combustion and Flame*, 34, pp. 213-214, 1979.

11. Odinstov, V.A., "Expansion of a Cylinder with Bottoms Under the Effect of Detonation Products," *Combustion, Explosion, and Shock Waves*, 27, pp. 94-97, 1991.

12. Kennedy, D.R., "The Elusive $\sqrt{2E}$," American Ordnance Association 21st Bomb and Warhead Section Meeting, Picatinny Arsenal, New Jersey, April 1969.

13. Zulkowski, T., *Development of Optimum Theoretical Warhead Design Criteriaa*, Naval Weapons Center, China Lake, California, NWC TP 5892, December 1976.

14. Kinney, G.F. and Graham, K.J., *Explosive Shocks in Air*, Springer-Verlag, New York, 1985.

15. Kingery, C.N. and Bulmash, G., *Airblast Parameters from TNT Spherical Air Burst and Hemispherical Surface Burst*, Ballistic Research Laboratory, Aberdeen Proving Ground, Maryland, ARBRL-TR-02555, Apr 1984.

16. Baker, W.E., *Explosions in Air*, Wilfred Baker Engineering (Second Printing of 1973 edition, 1983).

17. Swisdak, M.M., Jr., *Explosion Effects and Properties, Part 1 - Explosion Effects in Air*, Naval Surface Weapons Center, Silver Spring, Maryland, NSWC/WOL/TR 75-116, October 1975.

18. Petes, J., "Blast and Fragmentation Characteristics," Annals of the New York Academy of Sciences, *Prevention of and Protection Against Accidental Explosion of Munitions, Fuels and Other Hazardous Mixtures*, Vol. 152, Art. 1, pp. 283-316, October 28, 1968.

19. Swisdak, M.M., Jr., *Maximum TNT Equivalence of Naval Propellants*, Naval Surface Weapons Center, Silver Spring, Maryland, NSWC TR 83-120, February 1983.

20. Plooster, M.N., *Blast Effects from Cylindrical Explosive Charges: Experimental Measurements*, Naval Weapons Center, China Lake, California, NWC TP 6382, November 1982.

21. Held, M., "TNT – Equivalent," *Propellants, Explosives, Pyrotechnics*, 8, pp.158-167, 1983.

22. *Joint Munitions Effectiveness Manual*, USAF – 61A1-3-7; NAVY – NAVAIR 00-130-ASR-2-1; USMC – FMFM 5-21; ARMY – FM 101-51-3, Revision 2, 8 May 1989.

23. Victor, A.C., "A Simple Method for Calculating Shock Initiation of Explosives by Projectile Impact," 1993 JANNAF Propulsion Systems Hazards Subcommittee Meeting, Fort Lewis, Washington, 11-13 May, 1993.

24. Victor, A.C., "A Simple Method for Calculating Sympathetic Detonation of Munitions," 1993 JANNAF Propulsion Systems Hazards Subcommittee Meeting, Fort Lewis, Washington, 11-13 May, 1993.

25. Sewell, G.G.S. and Kinney, G.F., "Response of Structures to Blast: A New Criterion, Annals of the New York Academy of Sciences, *Prevention of and Protection Against Accidental Explosion of Munitions, Fuels and Other Hazardous Mixtures*, Vol. 152, Art. 1, pp. 532-547, October 28, 1968.

26. Dobbs, N., Cohen, E. and Weissman, S., "Blast Pressures and Impulse Loads for Use in the Design and Analysis of Explosive Storage and Manufacturing Facilities," ibid.

27. Taylor, W.J., "Blast Wave Behavior in Confined Regions," ibid.

28. Henrych, J., *The Dynamics of Explosion*, Elsevier, New York, 1979.

29. Baker, W.E., Westine, P.S. and Dodge, F.T., *Similarity Methods in Engineering Dynamics*, Spartan Books, Hayden Book Company, Rochelle Park, New Jersey, 1973.

30. Held, M., " Similarities of Shock Wave Damage in Air and Water," *Propellants, Explosives, Pyrotechnics*, 15, pp. 149-156, 1990.

31. Westine, P.S., "R-W Plane analysis of Vulnerability of Targets to Air Blast," *The Shock and Vibration Bulletin*, No. 42, Pt. 5, pp. 173-183 (1972).

32. Rinehart, J.S. and Pearson, J., *Behavior of Metals Under Impulsive Loads*, American Society for Metals, Scranton, Pennsylvania, 1954.

33. Young, W.C., *Roark's Formulas for Stress and Strain*, Sixth Edition, McGraw-Hill, New York, 1989.

34. Filler, W.S., "The Influence of Reactive Cases on Airblast from High Explosives," Proceedings of the Eighth Symposium (International) on Detonation, NSWC MP 86-194, pp. 207-208, 1985.

35. Filler, W.S., " The Influence of Inert Cases on Airblast," Proceedings of the Sixth Symposium (International) on Detonation, ACR-221, pp. 777-785, 1976.

36. Weibull, H.R.W., "Pressures Recorder in Partially Closed Chambers at Explosion of TNT Charges," Annals of the New York Academy of Sciences, *Prevention of and Protection Against Accidental Explosion of Munitions, Fuels and Other Hazardous Mixtures*, Vol. 152, Art. 1, pp. 356-351, October 28, 1968.

37. Kinney, G.F., Sewell, R.G.S., and Graham, K.J., *Peak Overpressures for Internal Blast*, Naval Weapons Center, China Lake, California, NWC TP 6089, June 1979.

38. Reinhardt, R.A., *Computations on Internal Blast From Titanium-Cased Charges in Air*, Naval Weapons Center, China Lake, California, NWC TP 6544, July 1984.

39. Athow, L.K., *Real Gas Considerations for Determining Physical and Thermodynamic Properties of Gases Involved in the Prediction of the Effects of Internal Explosions*, M.S. Thesis, Naval Postgraduate School, Monterey, California, June 1982.

40. Sewell, R.G.S., *Blast Overview and Near-Field Effects*, Naval Weapons Center, China Lake, California, NWC TM 3754, February 1979.

41. Baroody, E. and Peters, S., *Heats of Explosion, Heat of Detonation, and Reaction Products: Their Estimation and Relation to the First Law of Thermodynamics*, Indian Head, Maryland, NOS, IHTR 1340, May 1990.

42. Cruise, D.R., *Theoretical Computations of Equilibrium Composition, Thermodynamic Properties, and Performance Calculations of Propellant Systems*, Naval Weapons Center, China Lake, Calif, NWC TP 6037 Revision 1, November 1991.

43. Kinney, G.F. and Sewell, R.G.S., *Venting of Explosions*, Naval Weapons Center, China Lake, California, NWC TM 2448, July 1974.

44. Chanteret, P.Y., "Consideration about the Analytical Modelling of Shaped Charges," *Propellants, Explosives, Pyrotechnics*, 18, pp. 337-344, 1993. Also see V 18/5, pp. 241-306 of the same journal for additional related papers.

45. Carleone, J., *Tactical Missile Warheads*, AIAA, Progress in Astronautics and Aeronautics, Vol. 155, 1993.

46. Victor, A.C., "A Simple Method for Calculating Sympathetic Detonation of Cylindrical, Cased Explosive Charges," *Propellants, Explosives, Pyrotechnics*, 21, pp. 90-99, 1996.